J Nanostruct 12(4): 826-841, Autumn 2022

RESEARCH PAPER

Improvement of Corrosion and Osseointegration Characteristics for Ti6Al4V Alloy by Coating with Polyetheretherketone (Peek) And Nanohydroxyapatite Using Electrophoretic Deposition for Biomedical Applications

Muslim Idan Hamil, Khamael Ibrahim Abdulwahid, and Mundher AL-Shakban*

Department of Physics, College of Science, University of Misan, Maysan, Iraq

ARTICLE INFO

Article History:
Received 17 July 2022
Accepted 15 September 2022
Published 01 October 2022

Keywords:
Corrosion Ti6Al4V alloy
Electrophoretic
Nanohydroxyapatite
Polyetheretherketone

ABSTRACT

In this research Ti6Al4V alloy will coated with polyetheretherketone (PEEK) and nanohydroxyapatite composite. The coating will be achieved by electrophoretic deposition using solution a consist that of 1 gm PEEK and 6 gm nanohydroxyapatite in 50 ml of absolute ethanol and 0.2 gm iodine. The samples were deposited and immersed in SBF for5, 10, and15 minutes, then heat treated at 250 °C for 1hr. under air atmosphere in the furnace. The samples that will tested by X-Ray Diffraction (XRD) and Scanning Electron Microscopy (SEM) and corrosion test will include open circuit potential (OCP), polarization curve (tafel) and electrochemical impedance spectroscopy (EIS). The samples will be immersed in simulated body fluid (SBF) for 2 weeks. The sample will test by XRD and SEM and corrosion test and will include open circuit potential (OCP), polarization curve (tafel) and electrochemical impedance spectroscopy (EIS) again to evaluate the results of the osseointegration and corrosion characteristics.

How to cite this article
Hamil M I., Abdulwahid K I., AL-Shakban M. Improvement of Corrosion and Osseointegration Characteristics for Ti6Al4V Alloy by Coating with Polyetheretherketone (Peek) And Nanohydroxyapatite Using Electrophoretic Deposition for Biomedical Applications. J Nanostruct, 2022; 12(4):826-841. DOI: 10.22052/JNS.2022.04.005

INTRODUCTION

Due to the prevalence of accidents and armed conflict, metals and metal alloys play a significant role in the field of biomaterials as a means of repairing or replacing injured load-bearing bones[1, 2] . Due to their various benefits, including a high strength to weight ratio, good electrochemical corrosion resistance, low density, relatively low modulus of elasticity, and biological inertness, titanium and its alloys are widely employed in aerospace, automotive, and medical applications [3, 4]. Due to their excellent mechanical strength and ductility, titanium alloys Ti-6Al-4V are frequently utilized to create load-bearing hip implants and bone fixation devices[5]. This alloy is the most researched titanium alloy and demonstrates an excellent balance between strength and plastic characteristics [6, 7]. Due to a mismatch in stiffness between the implants and host bone, metallic implants also experience a stress shielding effect, which causes a loss in bone density [8]. Ceramics and polymers have been researched as potential bone substitute materials in this regard. Due to its striking resemblance to the mineral component of human bones, hydroxyapatite [$Ca_{10}(PO_4)_6(OH)_2$] is of particular interest. This is because it is already present in the bone's structure, as illustrated in Fig. 1 [9, 10].

* *Corresponding Author Email: dorkoosh@tums.ac.ir*

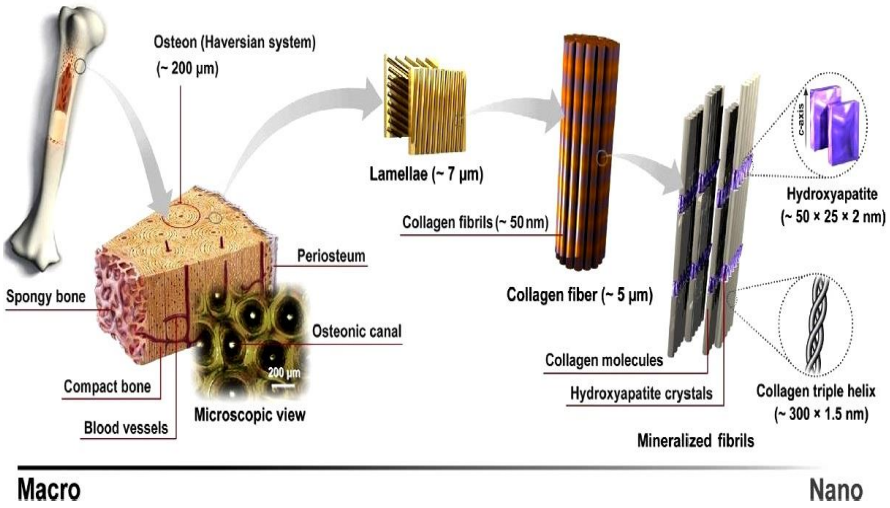

Fig. 1. Bones' hierarchical structure.

Bioactive, biocompatible, and osteoconductive bioceramic hydroxyapatite (HA) may adhere to natural bone[11, 12] . Due to its weak mechanical qualities and brittle structure, HA is mostly employed as a covering for implants and as bone filler [13]. However, due of its fragility, hydroxyapatite (HA) cannot be used for load-bearing implants. For biomedical applications, polymers with superior processability and low weight have advantageous properties.

Clinical uses for non-biodegradable polymers, such as polyetheretherketone (PEEK), include spinal cages, dental implants replacement, and high temperature durability and Young's modulus [14, 15]. In comparison to ceramic coatings, polyetherether-keton (PEEK) coatings are less stiff, which may help with the stress shielding problem [16]. However, PEEK's use in biological applications is constrained due to its bio-inter behavior [17]. According to the literature, PEEK's bioactivity and osteoconductive properties can be improved via coating, surface modification, and the creation of PEEK-based bioactive composites [18]. To create bioactive composites, hydroxyapatite (HA) can be deposited on PEEK or employed as a reinforcing material. The quantity of HA and PEEK in PEEK/HA composites affects their mechanical properties [19, 20].

The electrophoretic deposition (EPD) technique, which is used to coat medical implants,

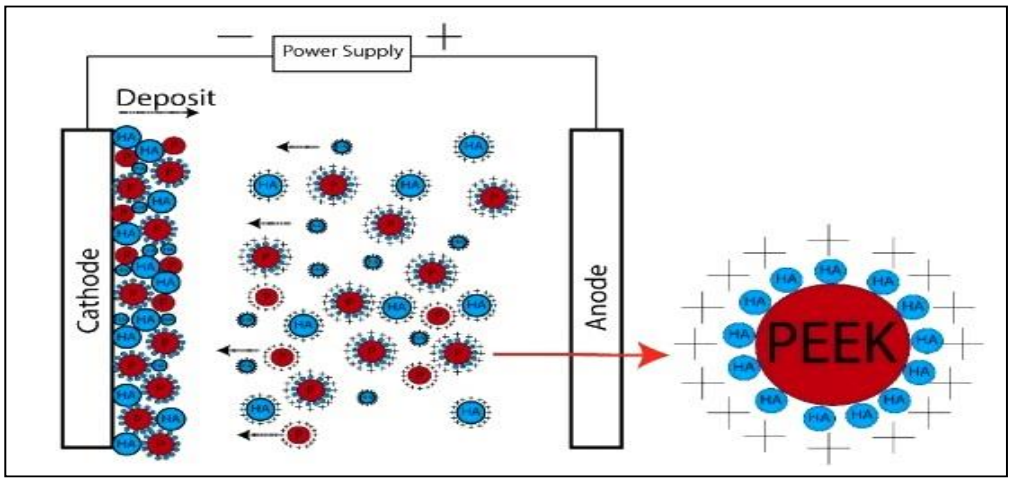

Fig. 2. Schematic representation of HA/PEEK electrophoretic deposition (EPD).

Table 1. Chemical composition of synthetic simulated body fluid (SBF)[30, 31].

ITEM	Description	Quantity gm/l
1	NaCl	8.036
2	KCl	0.225
3	$CaCl_2$	0.293
4	$NaHCO_3$	0.352
5	$K_2HPO_4.3H_2O$	0.230
6	$MgCl_2.6H_2O$	0.311
7	Na_2SO_4	0.072

is one of the common and significant choices for improving biocompatibility, as illustrated in Fig. 2 [21-23]. This method provides an even, medium-thick covering on the implant surface with good adherence. Additionally, it is one of the simple techniques that has been successfully utilized to cover medical implants.

Many researches dealt with coating hydroxyapatite on PEEK [24, 25] or coating PEEK and bioglass on medical implants [26, 27] or coating PEEK and graphite particle on medical implants. Some of research dealt with electrophoretic deposition of PEEK/graphene oxide suspension on medical implants [28]or electrophoretic deposition of PEEK- Gelatin on medical implants[29].

The advantage of this research was the investigate the electrophoretic deposition (EPD) of HA/PEEK nanocomposite coating on Ti-6Al-4V alloy substrates and to characterize coating characteristics like shape and phase's structure and attributes crucial for their potential bio applications including biocompatibility and osseointegration by biomimetic immersing in simulated body fluid (SBF) solution and corrosion behavior before and after immersing in (SBF) solution.

MATERIALS AND METHOD

Preparation of EPD suspension

The EPD suspension was prepared by adding 6 gm of nano hydroxyapatite (< 40 nm particle size, Skyspring Nanomaterials Inc.., USA) to 50 ml absolute ethanol 99.9% (Scharlau chemicals, Spain), then 0.5 gm PEEK resin powder99.9% (Nnochemazone, Canada) and 0.2 gm iodine crystals 99% (Mysiye labs, South Africa) were added to mixture. The mixture was stirred vigorously for 20 minutes to minimize the sedimentation.

Electrophoretic deposition on nano HA/PEEK particles on Ti-6Al-4V substrates

Ti-6Al-4V samples with (20×20×3) mm^3 were used as a substrate in this research. Samples were grinded by using 500 grit silicon carbide (SiC) papers. The samples were then cleaned by ethanol 96% (Scharlau chemicals, Spain) for 20 minutes twice using ultrasonic cleaner (1800 QT, 150W, China), then the samples were cleaned using distilled water one time for 20 minutes in the same ultrasonic cleaner. The Ti-6Al-4V alloys samples were coated by being connected as cathode to power supply (powerbox pacific ltd, New Zealand), graphite sheet (20 * 80) mm^2 were connected as anode. The distance between two electrodes was 15 mm and the voltage was applied at 30 V with time intervals 5, 10, and 15 minutes for each group of samples. After coating, the samples were heat treated at 250°C for 1 hr. before under air atmosphere using tubular furnace (Carbolite, England). The structure of the resulting powder after drying was evaluated by Fourier Transform infrared (FTIR) spectroscopy in the wave number range of 4000-400 cm^{-1}. The phase transformation was tested out by X-Ray diffraction analysis (Philips Geiger using Cu Ka, ƛ=1.5405 ^{0}A). The morphology of nano HA/PEEK particles were assessed by field-emission scanning electron microscopy (Vega TESCAN, Czech Republic). The corrosion behavior of (HA/PEEK) coating was investigated in synthetic simulated body fluid (SBF) solution which consists of chemical properties listed in

Table 1. using electrochemical potential stat (CHI 604E, China) where the open circuit potential (OCP), polarization curve (tafel) and electrochemical impedance spectroscopy test (EIS) was achieved.

Osseointegration and bioactivity test

In order to evaluate the osseointegration and bioactivity for coated samples, the samples were immersed in SBF solution for one month, then they were tested by XRD, FTIR AND FESEM. Also, the corrosion behavior for the coated samples was

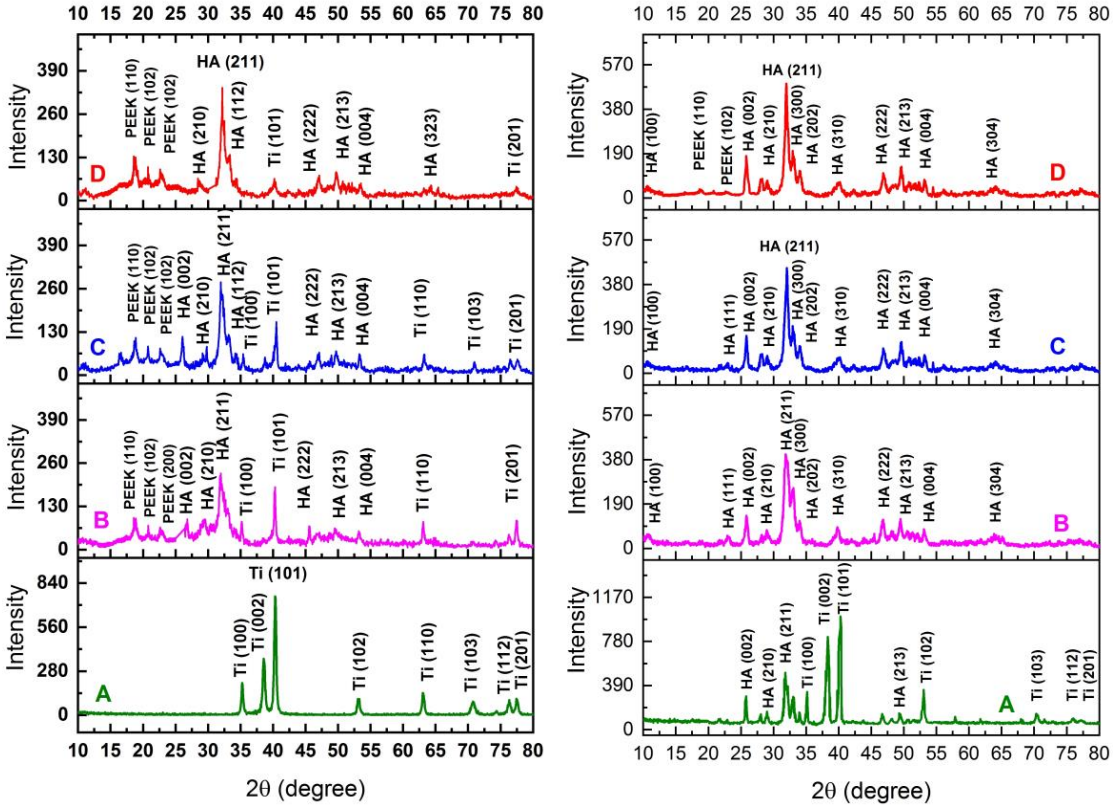

Fig. 3. XRD patterns of HA/PEEK coatings at 250°C for (B=5, C=10, and D= 15) minutes. (a) before immersion in SBF. (b) after immersion in SBF.

investigated after immersion.

RESULTS AND DISCUSSION

X-Ray Diffraction

The X-Ray diffraction analysis inspection was used to show the phase identification in HA/PEEK coating on Ti-6Al-4V alloy before and after immersion. Fig. 3 shows XRD pattern of the Ti-6Al-4V alloy coating with HA/PEEK at (5, 10. and 15) minutes. The XRD pattern of Ti can be seen in Fig. 3-a, the diffraction peaks at 2θ = 35.093, 38.421, 40.170, 53, 62.949, 70.661, 76.218, and 77.368° corresponding to (100), (002), (101), (102), (110), (103), (112), and (201) planes of titanium, while other materials of alloy did not appear, due to their percentages in the alloy. All the peaks are good agreement with JCPDS Card No JCPDS file #44-1294[30]. After coating, the intensity of Ti decreased with increasing of deposition time, spectrums (b, c, and d) in Fig. 3-b show XRD pattern for the HA/PEEK coating on Ti-6Al-4V alloy by electrophoretic deposition with different of deposition time. The XRD pattern identifies three peaks at 2θ =18.68, 20.74, and 22.92° corresponding to phases spectrum of PEEK at (110), (111), and (200). All the peaks of the XRD pattern of PEEK perfectly match with diffraction code 00-052-3277[31], while the peaks are 25.354, 28.966, 31,773, 32.196, 46.711, 48.103 and 53.143° for (002), (210), (211), (222), (213) and (004) agreement with JCPDS Card No. 09-0432 for nano hydroxyapatite. After immersing in SBF solution, we see the formation of a new layer of hydroxyapatite as an indicator of osseointegration behavior of coating layer. In titanium pattern a in Fig. 3-b, we see clearly the peaks at 2θ= 25.354, 28.966, 31,773, 32.196, 46.711, 48.103 and 53.143° corresponding to (002), (210), (211), (222), (213) and (004) planes are in agreement with JCPDS Card No. 09-0432 for nano hydroxyapatite. We see obviously from Fig. 2-b that the PEEK

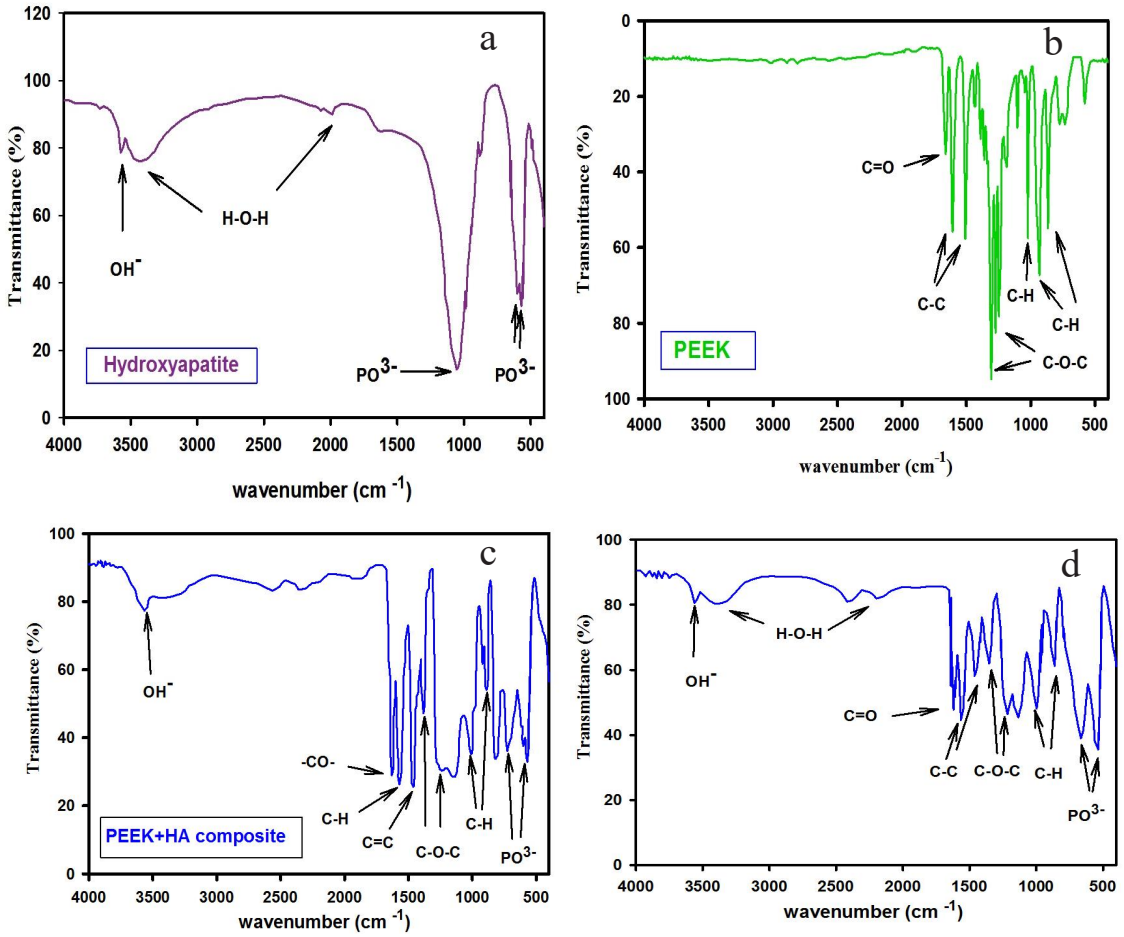

Fig. 4. a) FTIR spectrum of hydroxyapatite b) FTIR spectrum of polyetheretherketone (PEEK) c) FTIR spectrum of (HA-PEEK) composite coated Ti6Al4V alloy d) FTIR spectrum of (HA-PEEK) composite coated Ti6Al4V alloy after immersion in SBF solution for one month.

peaks in patterns (a, b and c) vanished except for two small peaks in pattern c at 2θ=18.68 and 22.92º corresponding to (110) and (102) planes, this happened because the hydroxyapatite formed from immersing in SBF solution covered the surface uniformly forming a thick layer which appears clearly in XRD test pattern and raises the intensity in hydroxyapatite peaks compared with that before immersing.

FTIR TEST

The chemical structure of HA, PEEK, (HA and PEEK composite) after coating and after immersion in SBF solution was examined by Fourier transform infrared spectra (Bruker, Canada), using the KB replete method at 400–4000 cm^{-1} wavelength. FTIR spectrum of hydroxyapatite in Fig. 4a shows the bands at 563.12 and 617.43 cm^{-1} were due to the flexural vibrations of the P–O bonds in the crystalline phosphate phase (PO^{3-}). The peak at1051.72 cm^{-1} corresponded to the stretching vibrations of P–O bonds. Ion stretching vibration around 2004.35,3422.27 and 3574.23 cm^{-1} confirms the presence of hydroxyl group (OH^-).

The FTIR spectrum for PEEK in Fig. 4b shows aromatic hydrogen's out of plane C-H bond bending modes occurred at 861.63 $cm^{-1}$and aromatic hydrogen C-H bonds in-plane deformation at 937.69 and 1021.37 cm^{-1}. The asymmetric stretching of ether group (C-O-C) appears at 1272.15 and 1296.89 cm^{-1}. The peaks at 1509.04 and 1608.85cm^{-1} are attributed to the in-plane vibration spectrum of the C–C bonds in the aromatic rings. The band at 1661.49 cm^{-1} belongs

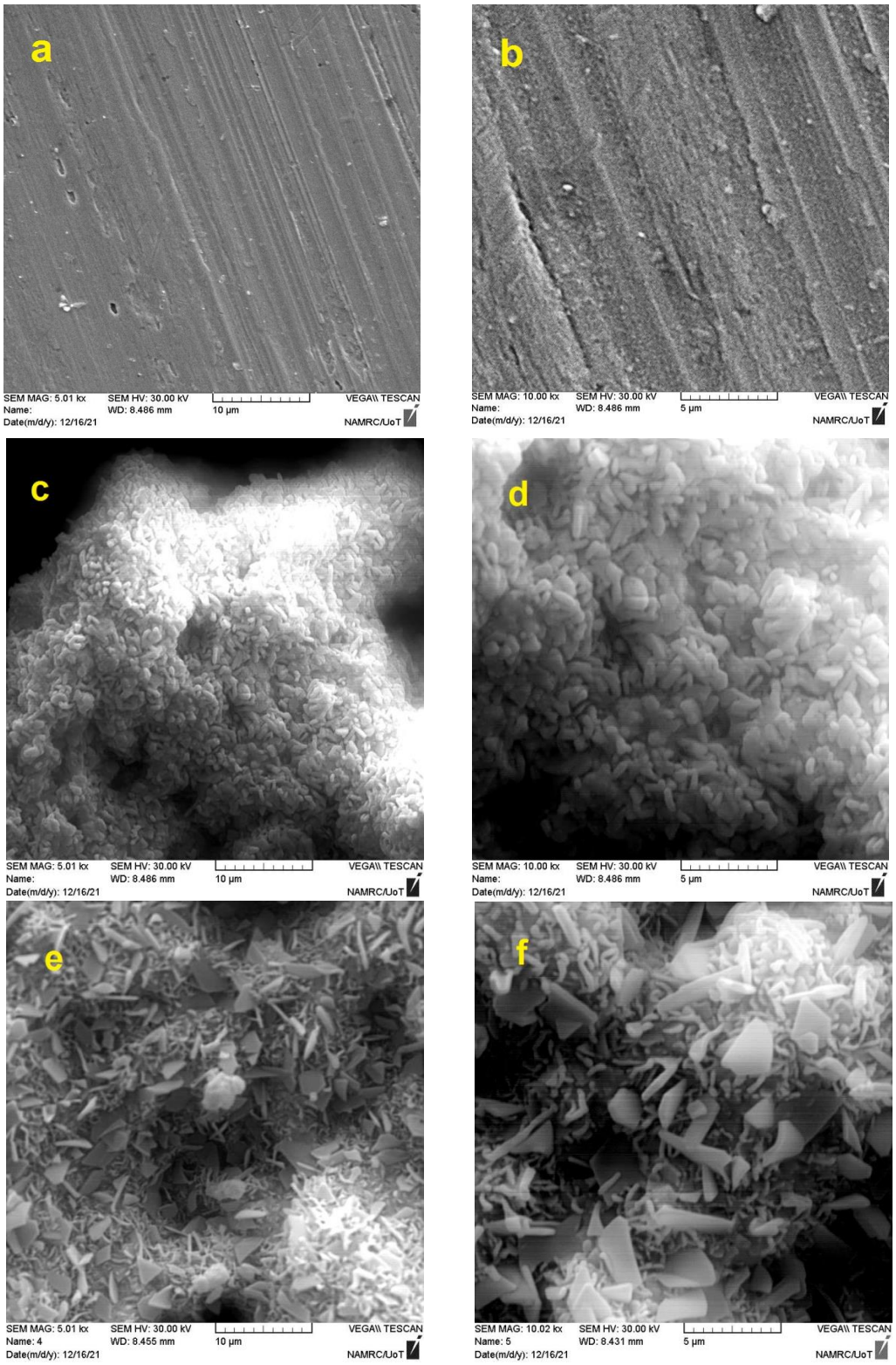

Fig. 5. SEM images for (HA and PEEK composite) coated on the surface of Ti6Al4V samples a, b: uncoated, c, d: 5 min. coated, e, f: 10 min. coated and g, h: 15 min coated.

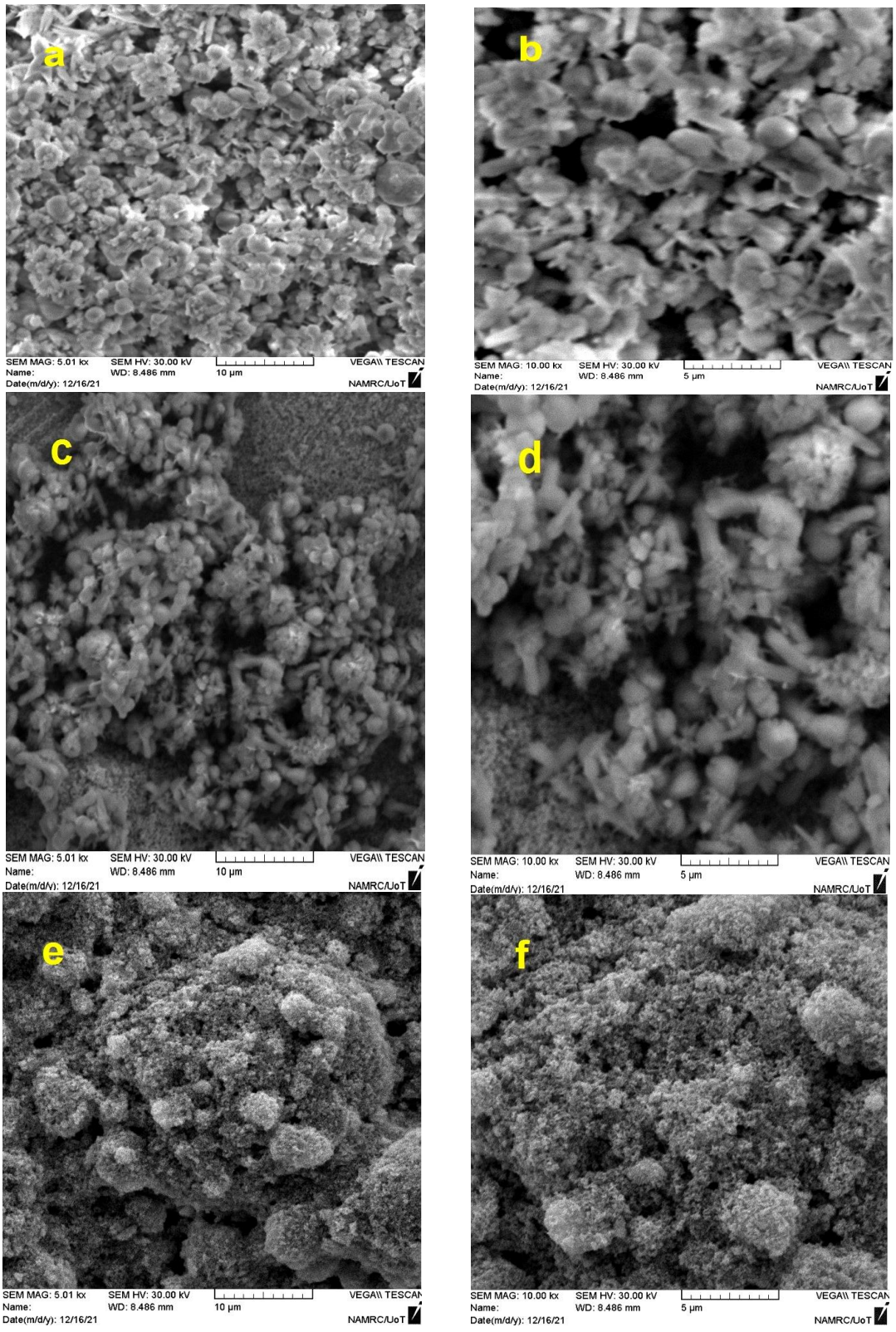

Fig. 6. SEM images for (HA and PEEK composite) coated on the surface of Ti6Al4V samples after immersion in SBF solution for one month a, b: uncoated, c, d: 5 min. coated, e, f: 10 min. coated and g, h: 15 min coated.

to the stretching vibration of the C=O functional group.

The FTIR spectrum of (HA-PEEK) layer coated Ti6Al4V alloy didn't show any chemical reaction or a new bond as shown in Fig. 4c. The FTIR spectrum shows the bands at 567.47 and 687.51 cm^{-1} were due to vibrations of the P–O bonds in the crystalline phosphate phase (PO^{3-}). The aromatic hydrogen's out of plane C-H bond bending modes was at 898.92 cm^{-1} and aromatic hydrogen C-H bonds in-plane deformation at 113.78 cm^{-1}. The asymmetric stretching of ether group(C-O-C) appears at 1226.31 and 1379.56 cm^{-1}. The peaks at 1465.714 and 1577.94 cm^{-1} are attributed to the in-plane vibration spectrum of the C–C bonds in the aromatic rings. The band at 1631.76 cm^{-1} belongs to the stretching vibration of the C=O functional group. The ion stretching vibration around 2032.17,3364.62 and 3550.89 cm^{-1} confirms the presence of hydroxyl group (OH^{-}).

The FTIR of the (HA-PEEK) composite coatedTi6Al4V alloy after immersing in SBF solution for one month also didn't show any change in chemical bonds, but the height of polyeteretherketone peaks be less than before, this happened because the new layer of hydroxyapatite increases the quantity of hydroxyapatite in the composite as shown on Fig. 4d.

SEM TEST

Fig. 5a-h showed the SEM images with different magnifications of the (HA and PEEK composite) coated on the surface of Ti6Al4V samples. As shown in the images, HA particles with micron sizes agglomerates on the surface of samples.

After immersing in SBF solution the SEM images with different magnifications in Fig. 6a-h show different morphology for hydroxyapatite formed from SBF solution. The coated samples show high agglomeration of fine micron size particles, and the formed particles become finer by increasing the coating time while the hydroxyapatite formed on the uncoated samples was relatively greater than the coated samples. These results confirm the previous results from XRD test that the coating layer enhances this integration behavior.

Wettability (contact angel) test

In order to evaluate how the coated alloy will be affected by simulated body fluid, the wettability contact angel was measured. In the Fig .7a and Fig. 7b and Table 2. the contact angel varies widely between uncoated base alloy and the 15 min. coated one where the value of the contact angle decreased significantly from 61.76º for uncoated alloy to 24.64º for 15 min coated sample. After immersion in SBF solution, the formed hydroxyapatite new layer plays a big role in reduction of contact angel 19.90º for uncoated base alloy to 0.0º for both 10 min. and 15 min coated samples. This means that the more the coating thickness increased, the more liquids will be absorbed and the contact angle will be reduced.

Electrochemical corrosion test

Corrosion performance of the HA and PEEK coating was investigated by using open circuit measurement (OCP), polarization curve (Tafel) and electrochemical impedance spectroscopy EIS analysis. The values of corrosion potential ($E_{corr.}$) and corrosion current density (i_{corr})were obtained by the extrapolation of the Tafel plot.

The OCP curve forTi6Al4V samples coated with (HA and PEEK composite) before immersion in SBF solution shows an increase in OCP value towards the positive side that's mean be more passive. The OCP enhanced from -0.296 volt for uncoated sample to -0.213 volt for that coated at 15 minutes as shown in Fig. 8a and Table 3.

After immersion in SBF solution, all samples

Table2. Wettability contact angel test results.

ITEM	Angel (dgree)
Base uncoated	61.79
5 min.	44.11
10 min.	35.16
15 min.	24.64
After immersing	
Base uncoated	19.90
5 min.	10.26
10 min.	0.0
15 min.	0.0

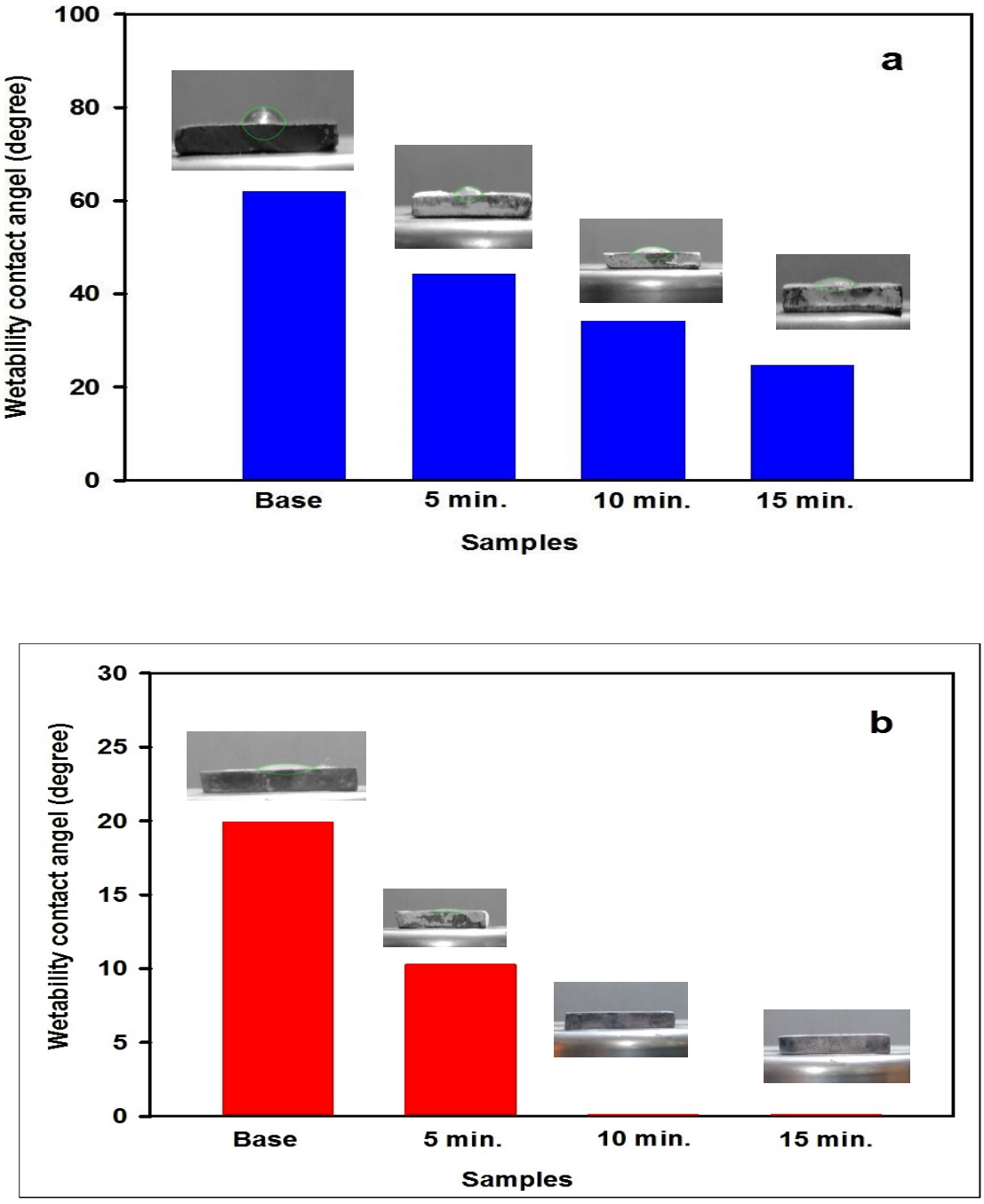

Fig. 7. Wettability contact angel test results for coated samples a: before immersion in SBF solution, b: after immersion in SBF solution.

become more passive and the OCP value decreased because the new hydroxyapatite layer formed from SBF solution covered the composite coated layer. The OCP reduced from -0.238 volt for uncoated sample to -0.187 volt for sample coated at 15 minutes as shown in Fig. 8b and Table 4.

The polarization curve (tafel) test for Ti6Al4V samples coated with (HA and PEEK composite) before immersion in SBF solution shows clear improvement in corrosion resistance, where the corrosion rate decreased from 2.346×10^{-2}mmpy for uncoated sample to 3.040×10^{-3} mmpy for that

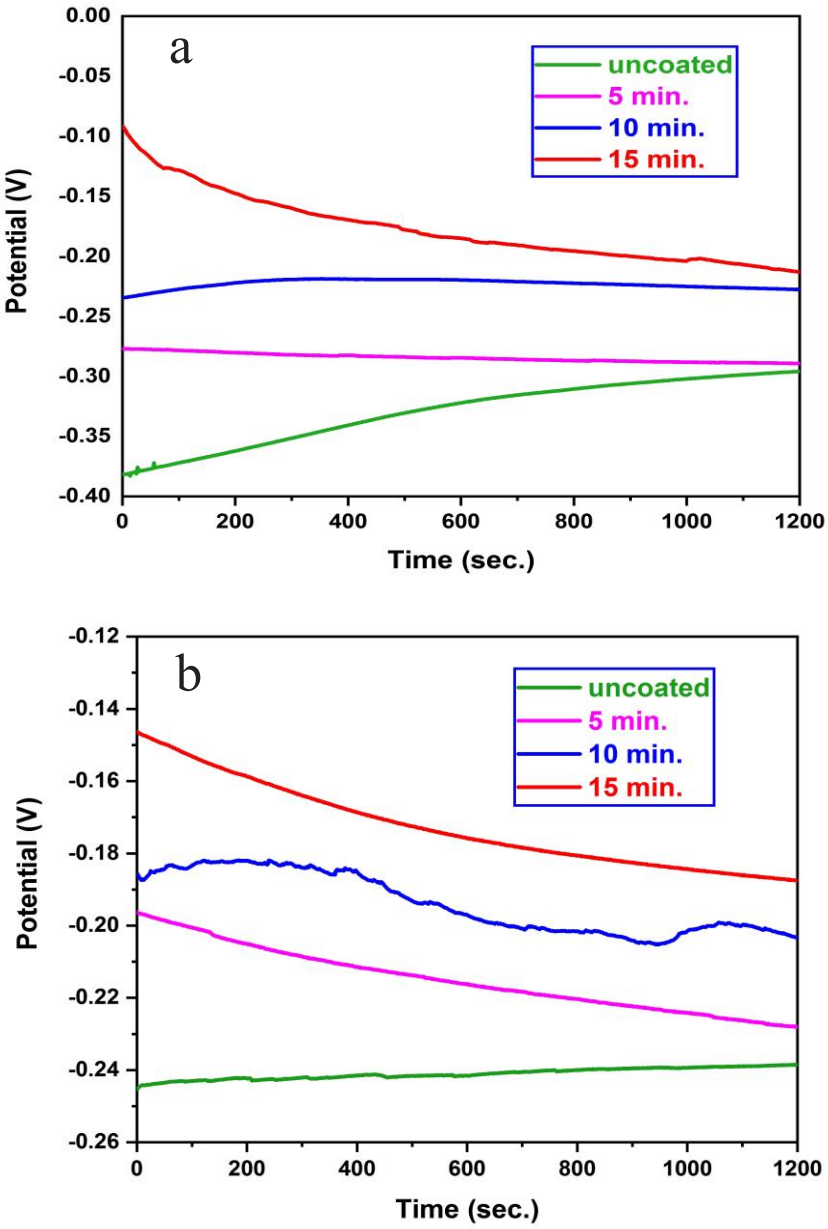

Fig. 8a. OCP measurement for Ti6Al4V samples coated with (HA and PEEK composite) before immersion in SBF solution b) OCP measurement for Ti6Al4V samples coated with (HA and PEEK composite) after immersion in SBF solution.

coated at 15 minutes. As shown in Fig. 9a and Table 5.

After immersion in SBF solution, the corrosion resistance obviously improved where the corrosion rate reduced from 1.369×10^{-2} mmpy for uncoated sample to 7.969×10^{-4} mmpy for 15 min. coated sample. This means we reduced the corrosion rate about 29 times compared with the sample uncoated and before immersing in SBF solution as shown in Fig. 9b and Table 6.

The polarization resistance could be determined by the following equation [32, 33]:

$$R_P = \frac{1}{2303 * i_{corr}} * \left(\frac{\beta_a * \beta_C}{\beta_a + \beta_C}\right) \quad (1)$$

R_p: the corrosion resistance in ohms cm^2.

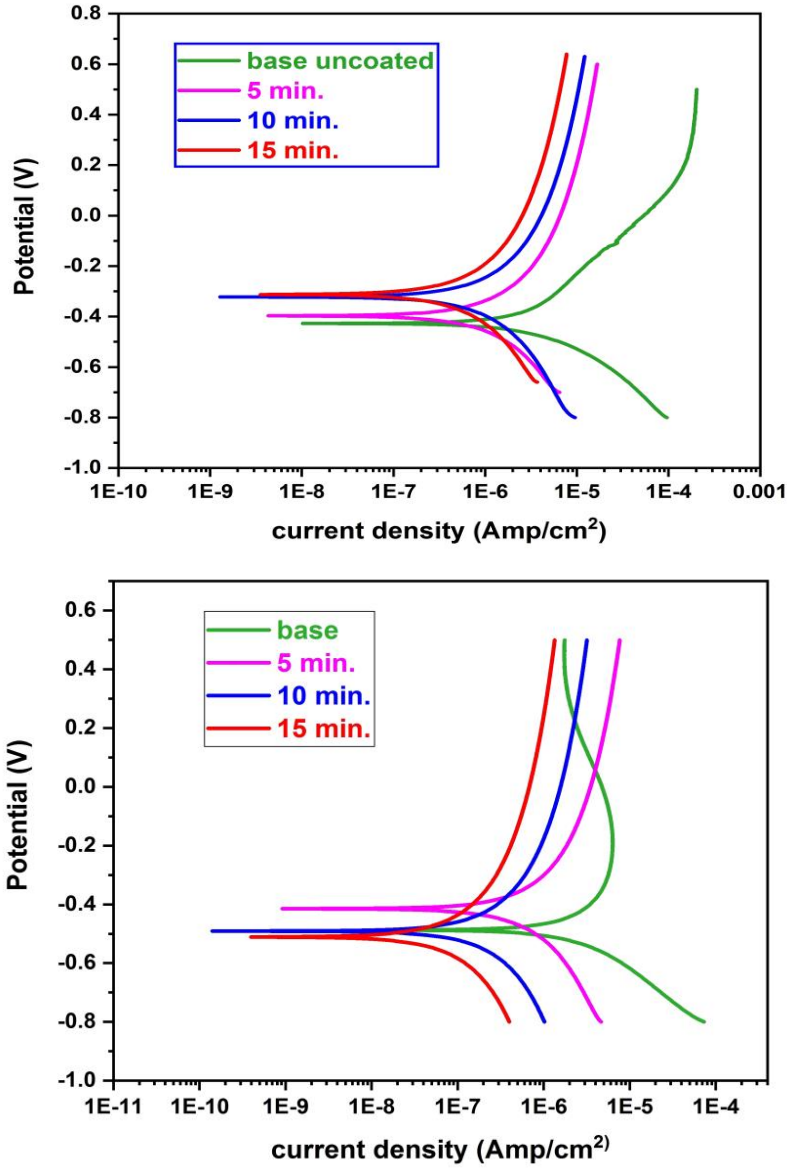

Fig. 9. a) polarization curve (tafel) for Ti6Al4V samples coated with (HA and PEEK composite) before immersion in SBF solution b) polarization curve (tafel) for Ti6Al4V samples coated with (HA and PEEK composite) after immersion in SBF solution.

i_{corr}: The corrosion current density on Amp/cm^2.

β_α: The anodic Tafel slope in volts/decade or mV/decade current density.

β_c: The cathode Tafel slope in volts/decade or mV/decade current density.

The quantity ($\beta_\alpha * \beta_c / \beta_\alpha + \beta_c$) is referred to as the Tafel constant.

Also, the protection efficiency can be determined using the equation [34]:

$$PE\% = \frac{(i\ corr.)uncoated - (\ icorr.)coated}{(i\ corr.)uncoated} \times 100 \qquad (2)$$

Where PE is the protection efficiency.

From Table 7. we see that the resistance of polarization increased with increasing coating time for samples before immersing in SBF solution and reached125 (ohm.cm^2) for sample coated at 15 minutes compared with 15.3 (ohm.cm^2) for uncoated one. Also, the protection efficiency

Table 3. OCP for Ti6Al4V samples coated with (HA and PEEK composite) before immersion in SBF solution.

ITEM	OCP (volt)
Base (uncoated)	-0.296
5 min.	-0.289
10 min.	-0.227
15 min.	-0.213

Table 4. OCP for Ti6Al4V samples coated with (HA and PEEK composite) after immersion in SBF solution.

ITEM	OCP (volt)
Base	-0.238
5 min.	-0.228
10 min.	-0.203
15 min.	-0.187

Table 5. corrosion characteristics for Ti6Al4V samples coated with (HA and PEEK composite) before immersion in SBF solution.

ITEM	Ecorr. (volt)	Icorr. (Amp)	Corr rate (mmpy)	βa	βc
Base (uncoated)	-0.424	2.735×10^{-6}	2.346×10^{-2}	0.151	0.265
5 min.	-0.397	7.194×10^{-7}	6.225×10^{-3}	0.545	0.199
10 min.	-0.322	4.988×10^{-7}	4.315×10^{-3}	0.203	0.206
15 min.	-0.313	3.514×10^{-7}	3.040×10^{-3}	0.198	0.208

Table 6. corrosion characteristics for Ti6Al4V samples coated with (HA and PEEK composite) after immersion in SBF solution.

ITEM	Ecorr. (volt)	Icorr. (Amp)	Corr rate (mmpy)	βa	βc
Base	-0.488	1.583×10^{-6}	1.369×10^{-2}	0.158	0.268
5 min.	-0.415	4.909×10^{-7}	3.837×10^{-3}	0.196	0.206
10 min.	-0.491	1.497×10^{-7}	1.694×10^{-3}	0.254	0.206
15 min.	-0.511	9.157×10^{-8}	7.969×10^{-4}	0.202	0.209

Table 7. the determined characteristics for Ti6Al4V samples coated with (HA and PEEK composite) before and after immersion in SBF solution.

ITEM	Before immersion		After immersion	
	Rp (ohm.cm^2)	PE %	Rp (ohm.cm^2)	PE %
Base	15.3	---------	27.3	42.12
5 min.	88.1	73.69	89.0	82.05
10 min.	89.0	81.76	330.0	94.52
15 min.	125.5	87.15	487.0	96.65

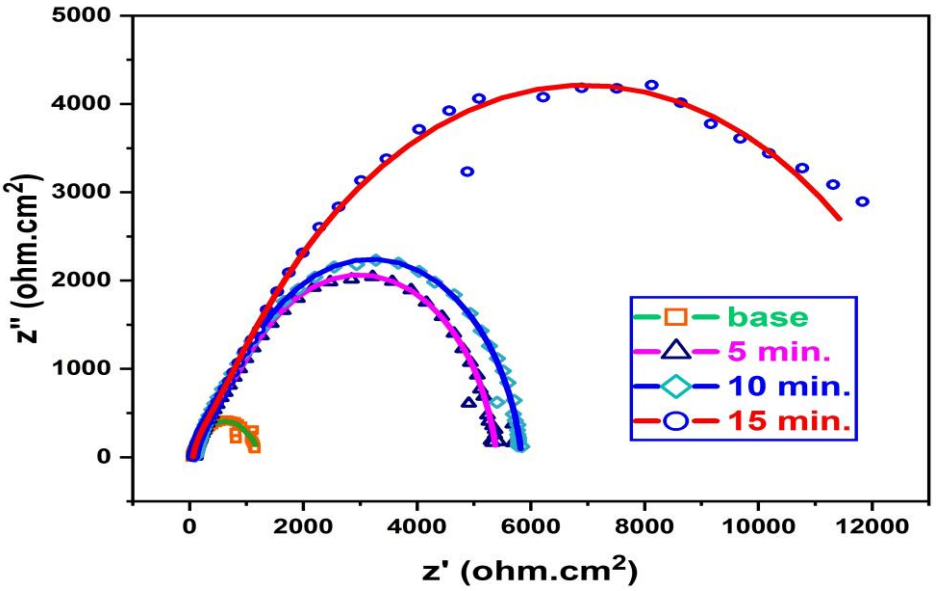

Fig. 10. Nyquist plots for Ti6Al4V samples coated with (HA and PEEK composite) before immersion in SBF solution.

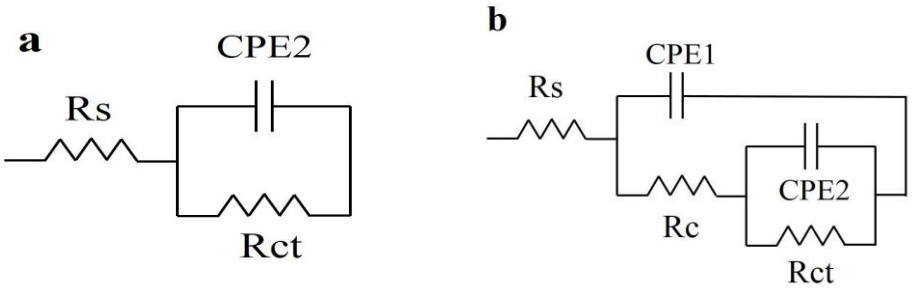

Fig. 11. Equivalent circuit used for fitting Nyquist data.

Table 8. electrochemical impedance spectroscope EIS results for coated alloy samples before immersion in SBF solution.

ITEM	R_S (OHM)	R_{c1} (ohm)	CPE_{c1} (F)	n1	R_{c2} (ohm)	CPE_{c2} (F)	n2
Base (uncoated)	41.16	1961.1	5.1833×10^{-5}	0.788	624.2	5.863×10^{-5}	0.838
5 min.	163.01	2608.6	3.753×10^{-5}	0.579	1997.7	4.636×10^{-5}	0.628
10 min.	171.3	6568.7	1.795×10^{-5}	0.651	3374.6	1.262×10^{-5}	0.858
15 min.	189.28	21699.3	2.870×10^{-6}	0.645	4464.2	7.320×10^{-6}	0.808

increased to reach 87.15% for sample coated at 15 minutes. After immersion in SBF solution, the resistance of polarization was significantly increased to reach 487 (ohm.cm^2) for sample coated at 15 minutes because of the new hydroxyapatite layer formed from SBF solution, and the protection efficiency reaches to 96.65 for the same sample.

In order to procure further inquiry related to the mechanism for coated layer corrosion resistance behavior before and after immersion in SBF solution, electrochemical impedance spectroscopy EIS experiments were performed.

From Nyquist plots in Fig. 10, we see a typical

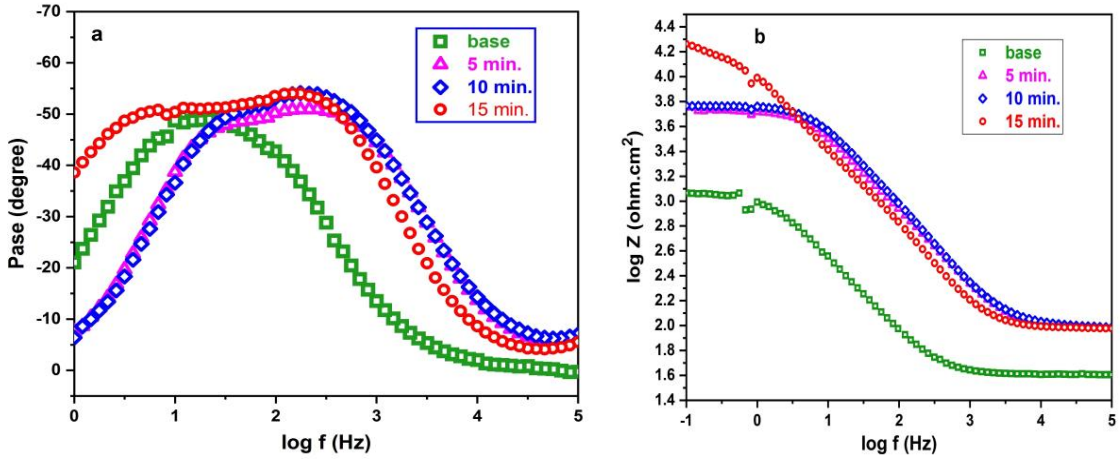

Fig. 12. bodes plots for Ti6Al4V samples coated with (HA and PEEK composite) before immersion in SBF solution.

Table 9. electrochemical impedance spectroscope EIS results for coated alloy samples before immersion in SBF solution.

ITEM	R_S (OHM)	R_c (ohm)	CPE_c (F)	n1	R_{dl} (ohm)	CPE_{dl} (F)	n2
Base(uncoated)	39.427	----------	----------	--------	1194.3	1.705×10^{-4}	0.757
5 min.	103.84	3597.2	3.319×10^{-6}	0.864	1701	4.319×10^{-6}	0.939
10 min.	107.87	3753.5	2.768×10^{-6}	0.883	1978.7	3.968×10^{-6}	0.917
15 min.	109.67	12608	2.729×10^{-5}	0.687	1996.7	3.706×10^{-6}	0.685

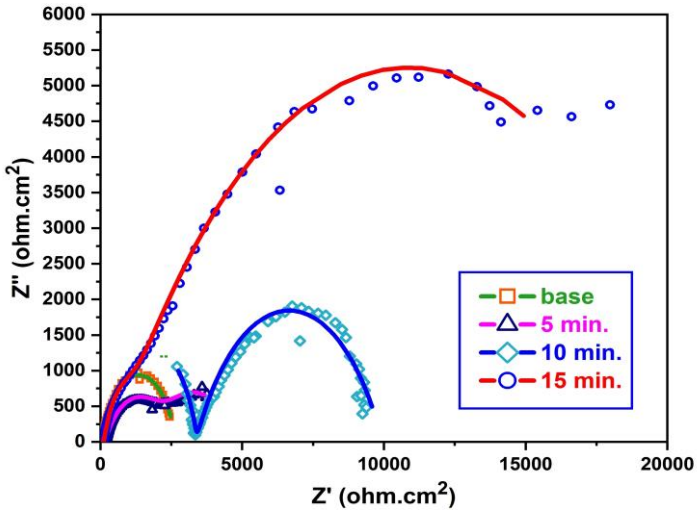

Fig. 13. Nyquist plots for Ti6Al4V samples coated with (HA and PEEK composite) after immersion in SBF solution.

closed semicircular shape expanding in diameter with increasing coating time until sample which was coated at 15 minutes the shape was be open semicircular. The equivalent circuit used for fitting data was shown in Fig. 11, where in Fig. 11-a it was used to fit data for uncoated sample while in Fig. 11-b it was used to fit data for other samples where we use constant phase elementCPE_1instead of double layer Capacitor C_{dl} because C_{dl} does not ideally behave as a capacitor and CPE_2 as the

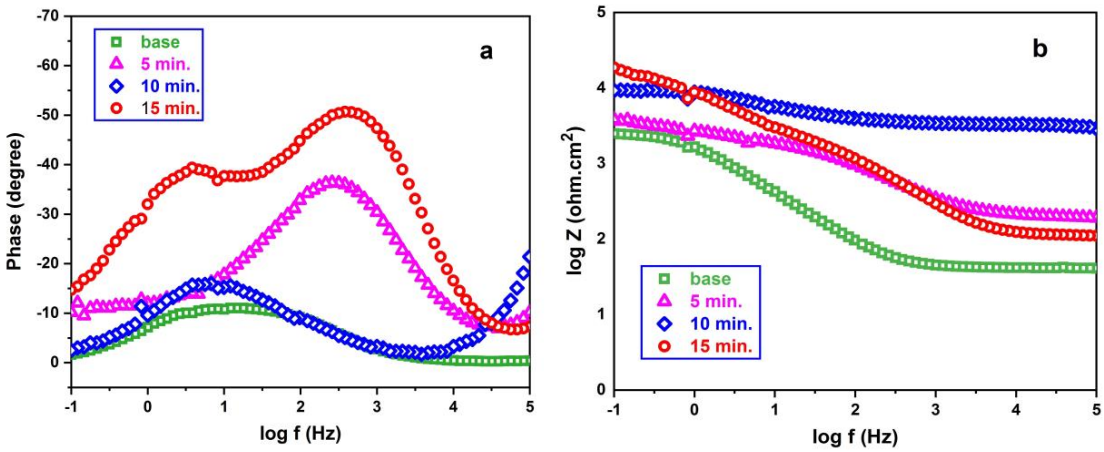

Fig. 14. bode plots for Ti6Al4V samples coated with (HA and PEEK composite) after immersion in SBF solution.

coated layer constant phase element. Also, we use R_S as the solution resistance, R_C as coated layer resistance and R_{ct} as the charge transfer resistance for double layer. We see from Table 8. how the CPEC increased with increasing coating time and reached12608.3(ohm.cm^2) compared with 1194.3(ohm.cm^2) for uncoated sample as an indication of the obvious effect of the coating layer in increasing the corrosion resistance and impeding the solution from reaching the surface of the alloy.

The bode plots for Ti6Al4V samples coated with (HA and PEEK composite) before immersion in SBF solution shows higher phase shift at low frequency, indicating a good passive coating in Bode Phase plot. And Bode |Z| plots show increasing in |Z| value in low frequency, indicating the enhancing of corrosion resistance with increasing coating time as shown in Fig. 12.

After immersion in SBF solution, Nyquist plots shows different shapes that attract attention, where all shapes except for uncoated sample shows two zones indicating the obvious effect of the new hydroxyapatite layer formed from SBF solution as shown in Fig. 13. The resistance R_C for the samples increased with increasing time to reach 21699.3 (ohm.cm^2) for that coated at 15 minutes. It is worth noting that the uncoated sample data also fitted using previous equivalent circuit in Fig. 11-b because it was also coated by the new layer of hydroxyapatite and its resistance reached1961.1 (ohm.cm^2) after immersion compared with 1194.3(ohm.cm^2) before immersion as shown in Table 9.

The bode plots for coated samples after immersing in SBF solution shows slight shift in Bode Phase plot at low frequency indicating a new enhancing in resistance because the new hydroxyapatite formed from SBF solution. Also bode |Z| plots show increasing in |Z| value in low frequency indicating the enhancing of corrosion resistance with increasing coating time as shown in Fig. 14.

CONCLUSION

From the previous results, we conclude that the increasing coating time increases the corrosion resistance and immersion in SBF solution for one month enhances osseointegration and corrosion behavior. The corrosion rate was reduced by about 29 times compared with the uncoated sample and protection efficiency reached 96.65 %. The EIS measurement shows an equivalent circuit for typical porous layer and this result is consistent with the SEM images test, the fitted results for coated layer after immersion in SBF solution reached21699.3(ohm.cm^2) compared with 1194.3(ohm.cm^2) for uncoated sample.

CONFLICT OF INTEREST

The authors declare that there is no conflict of interests regarding the publication of this manuscript.

REFERENCES

1. Azar V, Hashemi B, Rezaee Yazdi M. The effect of shot peening on fatigue and corrosion behavior of 316L stainless steel in Ringer's solution. Surf Coat Technol. 2010;204(21-22):3546-3551.

2. Gopi D, Ramya S, Rajeswari D, Kavitha L. Corrosion protection performance of porous strontium hydroxyapatite coating on polypyrrole coated 316L stainless steel. Colloids Surf B Biointerfaces. 2013;107:130-136.
3. Oh I-H, Nomura N, Masahashi N, Hanada S. Mechanical properties of porous titanium compacts prepared by powder sintering. Scripta Mater. 2003;49(12):1197-1202.
4. Niu QL, Zheng XH, Ming WW, Chen M. Friction and Wear Performance of Titanium Alloys against Tungsten Carbide under Dry Sliding and Water Lubrication. Tribology Transactions. 2013;56(1):101-108.
5. Lai W, Wang Y, Fu H, He J. Hydroxyapatite/polyetheretherketone nanocomposites for selective laser sintering: Thermal and mechanical performances. e-Polymers. 2020;20(1):542-549.
6. Muhammad M, Masoomi M, Torries B, Shamsaei N, Haghshenas M. Depth-sensing time-dependent response of additively manufactured Ti-6Al-4V alloy. Additive Manufacturing. 2018;24:37-46.
7. Peters M, Hemptenmacher J, Kumpfert J, Leyens C. Structure and Properties of Titanium and Titanium Alloys. Titanium and Titanium Alloys: Wiley-VCH Verlag GmbH & Co. KGaA; 2005. p. 1-36.
8. Khorasani AM, Goldberg M, Doeven EH, Littlefair G. Titanium in Biomedical Applications—Properties and Fabrication: A Review. Journal of Biomaterials and Tissue Engineering. 2015;5(8):593-619.
9. Alhussein Arkan M, Ismail Z, Che Nor Aiza J, Alsailawi HA, Mohammad Zorah H, Mustafa M, et al. A Brief Review on Biomedical Applications of Hydroxyapatite Use as Fillers in Polymer. J Chem Chem Eng. 2019;13(3).
10. Senra MR, Marques MdFV. Synthetic Polymeric Materials for Bone Replacement. Journal of Composites Science. 2020;4(4):191.
11. Ergun C. Synthesis and characterization of machinable calcium phosphate/lanthanum phosphate composites. J Mater Process Technol. 2008;199(1-3):178-184.
12. Sadat-Shojai M, Khorasani M-T, Dinpanah-Khoshdargi E, Jamshidi A. Synthesis methods for nanosized hydroxyapatite with diverse structures. Acta Biomater. 2013;9(8):7591-7621.
13. Pattanayak DK, Rao BT, Mohan TRR. Calcium phosphate bioceramics and bioceramic composites. J Sol-Gel Sci Technol. 2010;59(3):432-447.
14. Vaezi M, Yang S. Extrusion-based additive manufacturing of PEEK for biomedical applications. Virtual and Physical Prototyping. 2015;10(3):123-135.
15. Song J, Liao Z, Shi H, Xiang D, Liu Y, Liu W, et al. Fretting Wear Study of PEEK-Based Composites for Bio-implant Application. Tribology Letters. 2017;65(4).
16. Seuss S, Heinloth M, Boccaccini AR. Development of bioactive composite coatings based on combination of PEEK, bioactive glass and Ag nanoparticles with antibacterial properties. Surf Coat Technol. 2016;301:100-105.
17. Zheng Y, Xiong C, Zhang L. Formation of bone-like apatite on plasma-carboxylated poly(etheretherketone) surface. Mater Lett. 2014;126:147-150.
18. Ma R, Tang T. Current Strategies to Improve the Bioactivity of PEEK. Int J Mol Sci. 2014;15(4):5426-5445.
19. Abu Bakar MS, Cheang P, Khor KA. Mechanical properties of injection molded hydroxyapatite-polyetheretherketone biocomposites. Composites Science and Technology. 2003;63(3-4):421-425.
20. Abu Bakar MS, Cheang P, Khor KA. Tensile properties and microstructural analysis of spheroidized hydroxyapatite–poly (etheretherketone) biocomposites. Materials Science and Engineering: A. 2003;345(1-2):55-63.
21. Sak A, Moskalewicz T, Zimowski S, Cieniek Ł, Dubiel B, Radziszewska A, et al. Influence of polyetheretherketone coatings on the Ti–13Nb–13Zr titanium alloy's bio-tribological properties and corrosion resistance. Materials Science and Engineering: C. 2016;63:52-61.
22. Boccaccini AR, Keim S, Ma R, Li Y, Zhitomirsky I. Electrophoretic deposition of biomaterials. Journal of The Royal Society Interface. 2010;7(suppl_5).
23. Bartmański M, Pawłowski Ł, Strugała G, Mielewczyk-Gryń A, Zieliński A. Properties of Nanohydroxyapatite Coatings Doped with Nanocopper, Obtained by Electrophoretic Deposition on Ti13Zr13Nb Alloy. Materials. 2019;12(22):3741.
24. Johansson P, Jimbo R, Naito Y, Kjellin P, Currie F, Wennerberg A. Polyether ether ketone implants achieve increased bone fusion when coated with nano-sized hydroxyapatite: a histomorphometric study in rabbit bone. International Journal of Nanomedicine. 2016:1435.
25. Fiołek A, Zimowski S, Kopia A, Łukaszczyk A, Moskalewicz T. Electrophoretic Co-deposition of Polyetheretherketone and Graphite Particles: Microstructure, Electrochemical Corrosion Resistance, and Coating Adhesion to a Titanium Alloy. Materials. 2020;13(15):3251.
26. Boccaccini AR, Peters C, Roether JA, Eifler D, Misra SK, Minay EJ. Electrophoretic deposition of polyetheretherketone (PEEK) and PEEK/Bioglass® coatings on NiTi shape memory alloy wires. Journal of Materials Science. 2006;41(24):8152-8159.
27. Moskalewicz T, Zych A, Łukaszczyk A, Cholewa-Kowalska K, Kruk A, Dubiel B, et al. Electrophoretic Deposition, Microstructure, and Corrosion Resistance of Porous Sol–Gel Glass/Polyetheretherketone Coatings on the Ti-13Nb-13Zr Alloy. Metallurgical and Materials Transactions A. 2017;48(5):2660-2673.
28. González-Castillo EI, Costantini T, Shaffer MSP, Boccaccini AR. Nanocomposite coatings obtained by electrophoretic co-deposition of poly(etheretherketone)/graphene oxide suspensions. Journal of Materials Science. 2020;55(21):8881-8899.
29. Batool SA, Wadood A, Hussain SW, Yasir M, Ur Rehman MA. A Brief Insight to the Electrophoretic Deposition of PEEK-, Chitosan-, Gelatin-, and Zein-Based Composite Coatings for Biomedical Applications: Recent Developments and Challenges. Surfaces. 2021;4(3):205-239.
30. Klimova-Korsmik OG, Turichin GA, Shalnova SA, Gushchina MO, Cheverikin VV. Structure and properties of Ti-6Al-4V titanium alloy products obtained by direct laser deposition and subsequent heat treatment. Journal of Physics: Conference Series. 2018;1109:012061.
31. Abdulkareem MH, Abdalsalam AH, Bohan AJ. Influence of chitosan on the antibacterial activity of composite coating (PEEK /HAp) fabricated by electrophoretic deposition. Prog Org Coat. 2019;130:251-259.
32. Hamil M, Siyah M, Khalaf M. Electrophoretic deposition of Thin film TiO2 on Ti6AL4V alloy surface for biomedical applications. Egyptian Journal of Chemistry. 2020;0(0):0-0.
33. Hamil MI, Khalaf MK, Al-Shakban M. MAGNETRON SPUTTERED NANOCRYSTALLINE TiN THIN FILMS AND CORROSION PROPERTIES. Periódico Tchê Química. 2020;17(35):164-173.
34. Chen C, Mansfeld F. Corrosion protection of an Al 6092/SiC P metal matrix composite. Corros Sci. 1997;39(6):1075-1082.